MOL. PHOTOCHEM., 4(1), pp. 1-37 (1972)

Photoejection Dynamics [1]

RICHARD N. ZARE

Department of Chemistry
Columbia University
New York, New York

ABSTRACT

Semiclassical and quantum treatments of molecular photodissociation are presented in which it is shown that the angular distribution of the fragments will often be peaked parallel or perpendicular to the direction of the incident light beam. The form of the anisotropy is found to depend on the polarization of the light beam, the orientation of the electronic transition dipole moment within the molecule, and the dynamics of the dissociation process. A review is made of some recent experiments which exploit the angular distribution of photofragments to learn about the nature of the photejection process.

Copyright ©1972 by Marcel Dekker, Inc. **NO PART of this work may be reproduced or utilized in any form or by any means**, electronic or mechanical, including Xeroxing, photocopying, microfilm, and recording, or by any information storage and retrieval system, without permission in writing from the publisher.

INTRODUCTION

Few things in life improve with age; perhaps, only the great wines of Bordeaux. However, it is hoped that another exception may be made when one reflects on one's thesis. This paper is concerned with work [2] started by the author when he was a graduate student under the direction of Professor Dudley R. Herschbach of Harvard University.

In most photodissociation experiments the conditions of excitation of the molecules are so poorly defined that it is safe to assume that the molecules are bathed effectively in isotropic radiation and that there is no "state selection" or preferred orientation of the molecules for absorption. Indeed, this situation is so common that it is referred to as natural excitation in the literature [3]. However, if the excitation occurs in some definitely nonisotropic manner [4], such as by absorption from a unidirectional beam of light or by impacts from a beam of electrons or heavy particles, then the dynamics of the dissociation process can provide information about the interaction between the molecule and the exciting source.

Interest in the mechanics of molecular photodissociation has been stimulated by a number of recent experiments whose success depends on the nature of the primary photochemical step. For example, Dehmelt and co-workers [5] at the University of Washington have achieved molecular alignment by selective photodissociation; Kasper, Pimentel, and others [6] have achieved laser action by preparing an inverted medium through the photodissociation of polyatomic molecules; while Bersohn and co-workers [7] at Columbia University and Wilson and co-workers [8] at the University of California at San Diego have measured the angular distribution and velocity distribution of the recoiling photofragments from which they learn the symmetry nature of the repulsive electronic state and the partitioning of excess energy into internal and translational degrees of freedom. Moreover, the comparative study of photodissociation with other excitation processes such as electron impact often reveals striking similarities [2]. Since photodissociation is in general the simplest dissociative process, it is more amenable to exact calculation and its explication offers us a qualitative way for describing other more complex dissociative phenomena.

The Born-Oppenheimer and Franck-Condon principles allow a complete treatment and separation of the photoejection dynamics into angular and radial parts. According to the Franck-Condon principle [9], molecular transitions are most favored in which the position of the nuclei change little during the electronic jump which accompanies the absorption of a photon. Ordinarily, if the excited state dissociates, it does so in a time short compared to the rotational period of the molecule. Thus the distribution of the trajectories of

the fragments reflects the initial orientation of the molecule. The photodissociating molecules are not isotropically distributed with respect to the exciting light beam since the absorption probability is greatest when the transition dipole μ is aligned with the electric vector (polarization vector) ϵ of the light beam. Thus, the angular distribution of the fragments should show a corresponding anisotropy.

This paper is primarily concerned with the photodissociation of diatomic molecules, although the simple extension of many of these results to polyatomics is straightforward [2]. The calculation of the geometrical form factors that characterize the anisotropy amounts to averaging the angular dependence of the transition probability, proportional to $|\mu \cdot \epsilon|^2$, over all rotational orientations of the molecule. First, a semiclassical and then a quantum treatment of photoejection dynamics is given followed by a comparison of these predictions with the results of some recent experiments.

SEMICLASSICAL TREATMENT

Let us treat the motion of the electrons in the molecule by quantum mechanical principles whereas the motion of the nuclei is considered to be classical. Several distinct cases appear. These are specified by the polarization of the exciting light; by the orientation of the transition dipole μ with respect to the molecular framework; and by the direction of departure of the product fragments, which are regarded as undergoing either axial recoil along the initial direction of the molecular axis or transverse recoil perpendicular to it. If the photodissociation fragments separate with large excess kinetic energy, as is normally the case, then the trajectories of the fragments will be along the direction of the vibrational motion (axial recoil) of the ruptured bond. However, close to the threshold for photodissociation, the fragments have little excess kinetic energy and are ejected at right angles to the molecular axis by the rotational motion of the molecule (transverse recoil) like water spraying off a spinning wheel. The general result is readily synthesized from these two limiting cases for the recoil direction. The detailed weighting of axial and transverse recoil depends on the dynamical factors governing the photoejection process; the form of the angular distributions for axial or transverse recoil, however, is obtained from purely geometrical considerations.

Average Over Orientation Angles

The average over rotational orientations is conveniently formulated in terms of the Euler angles φ, θ, and ψ, shown in Fig. 1,

which relate the "molecule-fixed" set of coordinate axes g = x,y,z to the "space-fixed" system F = X,Y,Z with axes parallel to specified laboratory directions. For both coordinate frames, the origin is the

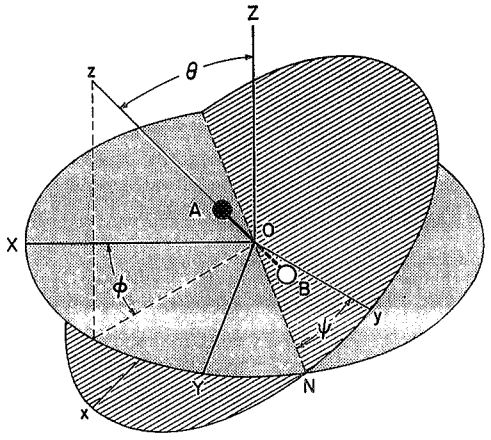

FIG. 1. Definition of Euler angles φ, θ, and ψ relating the space-fixed XYZ and molecule-fixed xyz coordinate systems. The angle θ is the included angle between Z and z, the angle φ is measured from the X axis to the projection of z upon the XY plane, and the angle ψ is measured from the line of nodes N, where the XYZ and xyz frames intersect, to the y axis. The internuclear axis of the AB molecule defines the z axis. The origin O of both coordinate systems is chosen to coincide with the center of mass of the AB molecule.

center of mass of the AB molecule. The angles θ and φ are ordinary polar coordinates that locate the z axis (chosen to lie along the internuclear axis of the molecule) relative to the Z axis and the XY plane, while ψ is an azimuthal angle measured about the z axis [10]. Since all orientations of the molecule are equally likely, $\sin\theta d\theta d\varphi d\psi$ is the (unnormalized) probability that the AB molecule is oriented with Euler angles in the range θ, φ, and ψ to $\theta + d\theta$, $\varphi + d\varphi$, and $\psi + d\psi$. If the electric vector ϵ has direction cosines λ_F along the space-fixed axes F and the transition dipole moment μ has direction cosines λ_g along the molecule-

fixed axes g, then the absorption probability is proportional to

$$|\mu \cdot \epsilon|^2 = \mu^2 \epsilon^2 |\Sigma_F \Sigma_g \lambda_F \lambda_g \Phi_{Fg}(\varphi,\theta,\psi)|^2 \quad (1)$$

where in obtaining Eq. (1) we have used the relations

$$\epsilon_F = \epsilon\lambda_F \quad (2)$$

$$\mu_g = \mu\lambda_g \quad (3)$$

and

$$\mu_F = \Sigma_g \Phi_{Fg} \mu_g \quad (4)$$

In Eq. (4) the angle-dependent factors Φ_{Fg} are the direction cosines, shown in Table 1, which describe the unitary transformation between the XYZ and xyz coordinate systems illustrated in Fig. 1.

TABLE 1

Direction Cosine Matrix Elements $\Phi_{Fg}(\varphi, \theta, \psi)$

	X[a]	Y[a]	Z[a]
x	$c\varphi c\theta c\psi - s\varphi s\psi$	$s\varphi c\theta c\psi + c\varphi s\psi$	$-s\theta c\psi$
y	$-c\varphi c\theta s\psi - s\varphi c\psi$	$-s\varphi c\theta s\psi + c\varphi c\psi$	$s\theta s\psi$
z	$c\varphi s\theta$	$s\varphi s\theta$	$c\theta$

[a]Here, sine is abbreviated by s, cosine by c.

The probability that dissociation occurs for an AB molecule oriented in the solid angle, $\sin\theta d\theta d\varphi d\psi$, is given by

$$P(\varphi,\theta,\psi)\sin\theta d\theta d\varphi d\psi = |\Sigma_F \Sigma_g \lambda_F \lambda_g \Phi_{Fg}(\varphi,\theta,\psi)|^2 \sin\theta d\theta d\varphi d\psi \quad (5)$$

Let us choose the z axis of the molecule-fixed system along the direction of departure of fragment A so that the polar coordinates describing the angular distribution of A in the center-of-mass system are identical to the Eulerian angles θ and φ (see Fig. 1). The relative flux that enters the solid angle element $\sin\theta d\theta d\varphi$ is given simply by averaging $P(\varphi,\theta,\psi)$ given by Eq. (5) over the

azimuthal angle ψ. By definition, this intensity is $I(\theta,\varphi)\ \sin\theta d\theta d\varphi$, where $I(\theta,\varphi)$ is the angular distribution. Therefore, we have

$$I(\theta,\varphi) = \frac{1}{2\pi}\int_0^{2\pi} |\Sigma_F \Sigma_g \lambda_F \lambda_g \Phi_{Fg}(\varphi,\theta,\psi)|^2\ d\psi \tag{6}$$

Equation (6) is a general expression for the angular distribution of the photofragments A and B assuming axial recoil. However, for most practical applications Eq. (6) is excessively general, i.e., its form may be greatly simplified by choosing the XYZ laboratory coordinates to be defined in terms of the light beam and by classifying the direction of μ in the xyz molecular frame based on symmetry arguments. For example, the FF' cross products in Eq. (6) disappear if one of the axes, say, the Z axis, is chosen to lie along the electric vector ϵ in the case of a beam of plane polarized light. The gg' cross products in Eq. (6) also disappear because of the orthogonality of the direction cosine matrix elements with respect to integration over ψ

$$\frac{1}{2\pi}\int_0^{2\pi} \Phi_{Fg}\,\Phi_{Fg'}\,d\psi = \frac{1}{2}\,\Phi^2_{Fg}\,\delta gg' \tag{7}$$

Thus, Eq. (6) reduces to a single term

$$I_{Fg}(\theta,\varphi) = \frac{1}{2\pi}\int_0^{2\pi} \Phi^2_{Fg}(\varphi,\theta,\psi)\,d\psi \tag{8}$$

or to a sum of such terms.

For a diatomic molecule, and for many other transitions of symmetrical polyatomic molecules [11], the transition dipole moment μ must either lie along the axis of the molecule corresponding to a parallel transition or lie in a plane at right angles to the molecular axis corresponding to a perpendicular transition. Thus, for parallel-type transitions such as Σ-Σ and Π-Π, $\mu_x = \mu_y = 0$ while $\mu_z \neq 0$, whereas for perpendicular-type transitions such as Σ-Π and Π-Δ, $\mu_x = \mu_y \neq 0$ while $\mu_z = 0$. For a beam of light with its electric vector pointing along the Z axis the angular distribution of the fragments for a parallel transition is given by

$$I_{Zz}(\theta,\varphi) = \frac{1}{2\pi}\int_0^{2\pi} \Phi^2_{Zz}(\varphi,\theta,\psi)\ d\psi = \cos^2\theta \tag{9}$$

and for a perpendicular transition by

$$I_{Zx} + I_{Zy} = \frac{1}{2\pi} \int_0^{2\pi} (\Phi^2_{Zx} + \Phi^2_{Zy})\, d\psi = \sin^2\theta \qquad (10)$$

In the case of an unpolarized light beam, it is convenient to choose the Z axis to lie along the direction of the light beam. The ϵ_X and ϵ_Y components of the electric vector are equal in magnitude and contribute independently since their relative phase is random. Thus, the angular distribution of the photodissociation products caused by an unpolarized light beam is given by

$$I_{\parallel}(\theta) = I_{Xz} + I_{Yz} \qquad (11)$$

for a parallel transition and

$$I_{\perp}(\theta) = I_{Xx} + I_{Xy} + I_{Yx} + I_{Yy} \qquad (12)$$

for a perpendicular transition. The same result applies to circularly polarized light since the rapid rotation of the electric vector is "averaged out" in a steady state experiment.

The photofragment angular distribution for transverse recoil are obtained by permuting the μ_g components $z \rightarrow x$ (or y), $x \rightarrow y$ (or z), and $y \rightarrow z$ (or x). In Table 2 formulas for the various cases are collected. These distributions have the form characteristic of a dipole radiation pattern

$$I(\theta) = 1/(4\pi)[1 + \beta P_2(\cos\theta)] \qquad (13)$$

where

$$P_2(\cos\theta) = \frac{3\cos^2\theta - 1}{2} \qquad (14)$$

We refer to β as the asymmetry parameter, and it ranges from $\beta = 2$, a cosine-squared distribution, to $\beta = -1$, a sine-squared distribution. The value $\beta = 0$ corresponds to an isotropic distribution. The differential cross sections satisfy the expected sum rules

$$\frac{1}{3} I_A(\theta) + \frac{2}{3} I_T(\theta) = 1 \qquad (15)$$

for axial (A) and transverse (T) recoil, and

$$\frac{1}{3} I_{\parallel}(\theta) + \frac{2}{3} I_{\perp}(\theta) = 1 \qquad (16)$$

TABLE 2

Angular Distribution of Photofragments $I(\theta) = [1 + \beta P_2 (\cos \theta)]/4\pi$ in terms of the asymmetry parameter β[a]

Electronic transition	Axial recoil	Transverse recoil
For plane polarized light with $\epsilon \parallel Z$:		
$\parallel$-type	$\beta = 2$	$\beta = -1$
$\perp$-type	$\beta = -1$	$\beta = \frac{1}{2}$
For unpolarized light incident along the Z axis:		
$\parallel$-type	$\beta = -1$	$\beta = \frac{1}{2}$
$\perp$-type	$\beta = \frac{1}{2}$	$\beta = -\frac{1}{4}$

[a]Here, $\int_0^{2\pi} \int_0^{\pi} I(\theta,\varphi) \sin \theta d\theta d\varphi = 1$.

for parallel ($\parallel$) and perpendicular ($\perp$) transitions. Note that the photofragment distributions for axial recoil peak at right angles to the incident light beam for parallel transitions and peak forward and backward along the light beam for perpendicular transitions. Figure 2 illustrates the forms of these anisotropic angular distributions where the Z axis has been chosen to bring out the symmetry of the distributions.

The generalization of these results to higher order multipole radiation is straightforward. For example, magnetic dipole transitions that result in photodissociation will yield the same angular distribution as in dissociative electric dipole transitions except that the former must be measured with respect to the magnetic vector rather than the electric vector of the light beam. In the most general case interference effects arise if both electric and magnetic multipole transitions both occur, e.g., magnetic dipole and electric quadrupole transitions. However, higher order multipole dissociative processes are expected to be so weak that they are seldom of much practical significance.

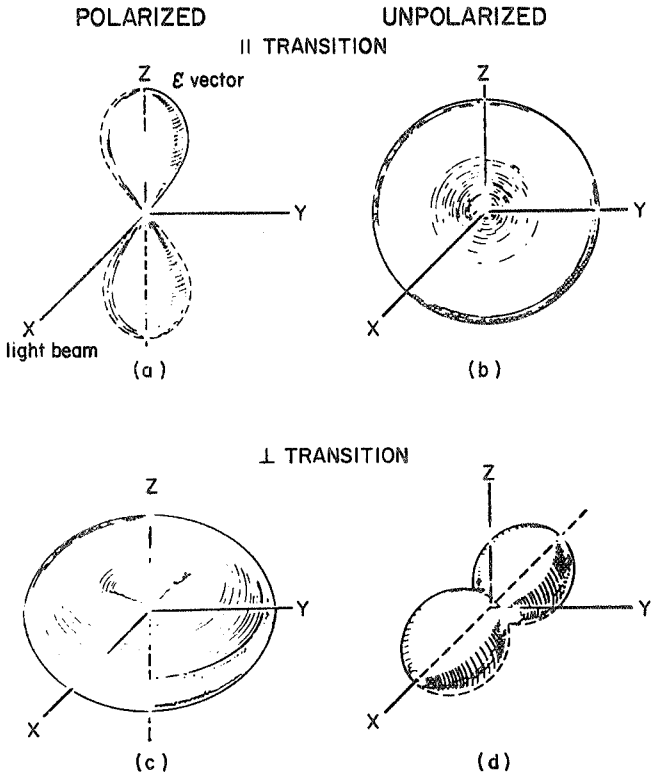

FIG. 2. Angular distribution of recoiling photofragments for the case of axial recoil. Cases (a) and (b) picture a parallel-type transition induced by plane polarized or unpolarized light, respectively. Cases (c) and (d) picture in a similar manner a perpendicular-type transition. In cases (a)-(d) corresponding to the four axial-recoil entires in Table 2 the light beam is incident along the X axis, and if plane polarized, the electric vector ϵ points along the Z axis.

The generalization of these results to photodissociation by multiphoton absorption processes is also straightforward. Let us restrict

our attention to two-photon photodissociation processes. The differential cross section may be obtained by a simple application of second-order perturbation theory. The result is

$$I(\theta,\varphi) = \left| \sum_{\psi_{int}} \frac{\langle \psi_f | \mu \cdot \epsilon | \psi_{int} \rangle \langle \psi_{int} | \mu \cdot \epsilon | \psi_i \rangle}{E_i - E_{int} + h\nu} \right|^2 \qquad (17)$$

where E_i and E_{int} are the energies of the initial and intermediate states, and the sum in Eq. (17) is to be performed over all intermediate states. Equation (17) is valid only for a two-photon nonresonant absorption process, i.e., the photon energy $h\nu$ does not lie within a natural width of any intermediate state, in which case the transition probability is proportional to the square of the intensity (the fourth power of the electric field) of the light beam. For a resonant two-photon absorption process, Eq. (17) formally diverges, but the angular distribution is still proportional to the numerator of this expression. In such a process, a steady state population is established in the (real as opposed to virtual) intermediate state. The angular distribution form factors are calculated classically by performing the average $\langle \Phi^2_{Fg} \Phi^2_{Fg'} \rangle$ and summing the result for all intermediate states. In most practical cases, the contribution of one of the intermediate states dominates. Table 3 summarizes the possible cases appropriate to photodissociation by a beam of linearly polarized light. It is to be noted, however, that unlike the one-photon case, two-photon photodissociation by circularly polarized or unpolarized light beams may give different angular distributions and different cross sections [12]. In any case, two-photon or higher multiphoton dissociation processes require intense light sources such as have now become available with the advent of powerful pulsed laser systems.

Effect of Rotational Motion

Unless the recoil velocity is very large compared to the angular velocity of molecular rotation, the angular distribution of products will be "smeared out" to some extent by the molecular rotation. As indicated in Fig. 3, the line joining the two separating fragments rotates from its initial direction at time $t = 0$, when the photon is absorbed, and approaches asymptotically ($t \to \infty$) a line that makes an angle θ_{max} with the initial direction. The recoil angle θ_{max} is

TABLE 3

Angular Distribution of Photofragments for a Two-Photon Dissociative Process Resulting from a Beam of Linearly Polarized Light[a]

Symmetry character of transition[b]	$I(\theta,\varphi)$[c]
$(\parallel, \parallel)$	$(5/4\pi)\cos^4\theta$
$(\parallel, \perp)$	$(15/8\pi)\cos^2\theta \sin^2\theta$
$(\perp, \parallel)$	$(15/8\pi)\cos^2\theta \sin^2\theta$
$(\perp, \perp)$	$(15/32\pi)\sin^4\theta$

[a] Axial recoil and the domination of one intermediate state is assumed. Here, $\int_0^{2\pi}\int_0^{\pi} I(\theta,\varphi)\sin\theta d\theta d\varphi = 1$.

[b] A $(\parallel, \parallel)$ transition refers to a two-photon transition in which the electric dipole transition between the initial state and the intermediate state is a parallel-type transition, and the electric dipole transition between the intermediate state and the final state is also a parallel-type, etc.

[c] The angular anisotropies are more pronounced in the two-photon $(\parallel, \parallel)$ and $(\perp,\perp)$ cases than their one-photon $(\parallel)$-type and $(\perp)$-type counterparts. However, the two-photon $(\parallel, \perp)$ or $(\perp, \parallel)$ transitions are cloverleaf-shaped, peaking at 45°, 135°, 225°, and 315° to ϵ.

obtained by considering the molecular photodissociation process as a "half-collision." By reversing the trajectory calculation for a two-body collision [13], we obtain

$$\theta_{max}(r_c, L) = (L^2/2\mu)^{\frac{1}{2}} \int_{r_c}^{\infty} \frac{dr/r^2}{[V(r_c) + L^2/2\mu r_c^2 - V(r) - L^2/2\mu r^2]^{\frac{1}{2}}} \tag{18}$$

where $V(r)$ is the repulsive potential of the dissociative electronic state, L is the rotational angular momentum of the molecule (which in spectroscopic work is traditionally denoted by J), and r_c is the

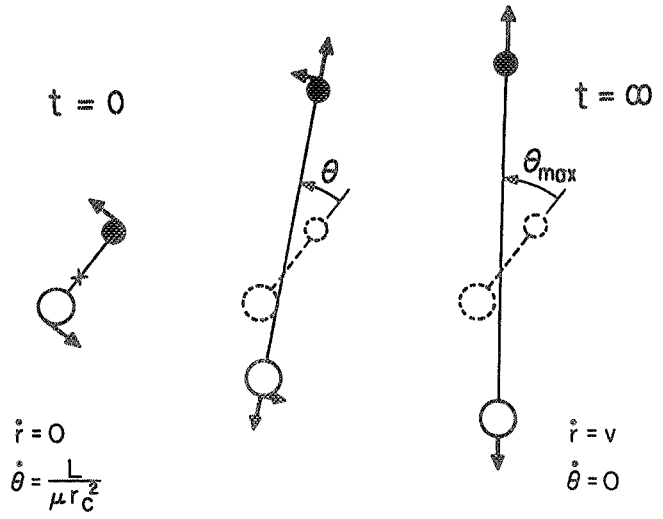

FIG. 3. Trajectory of recoiling photofragments. Initially (t = 0) the angular velocity $\dot{\theta}$ is classically given by L/2I where L is the rotational angular momentum of the molecule and $I = \frac{1}{2}\mu r_c$ is its moment of inertia at the internuclear spacing r_c. The radial velocity $\dot{r}$ initially is set to zero corresponding to the primitive classical approximation to the Franck-Condon principle in which the molecule makes an upward electronic transition only at the classical turning point (s) r_c of its vibrational motion in the ground state potential. Asymptotically ($t = \infty$) the angular velocity approaches zero and the radial velocity approaches its terminal value v. The recoil angle θ attains a large fraction of its asymptotic value θ_{max} during the short time the separating fragments are close to one another, say, within 10 Å of one another.

classical turning point of the trajectory, given by the initial internuclear separation of the recoiling fragments. The recoil angle θ_{max} is related to the more familiar classical deflection angle χ by the relation [13]

$$\chi = \pi - 2\theta_{max} \tag{19}$$

To obtain the angular distribution corresponding to a given θ_{max}, we introduce a new system of axes (see Fig. 4) denoted by $g_r = x_r, y_r, z_r$ (with r for "recoil"), where the z_r axis is chosen parallel to the asymptote of the trajectory. The old "molecule-fixed" system, denoted by $g_m = x_m, y_m, z_m$, has z_m along the molecular axis. Hence, as shown in Fig. 4, θ_{max} is the polar angle relating the g_r and g_m coordinate systems. We are at liberty to fix the positions of the remaining axes, x_m, x_r, y_m, and y_r. By choosing x_m to coincide with the projection of z_r upon the $x_m y_m$ plane, and by choosing y_r to coincide with the line of nodes (see Figs. 1 and 4),

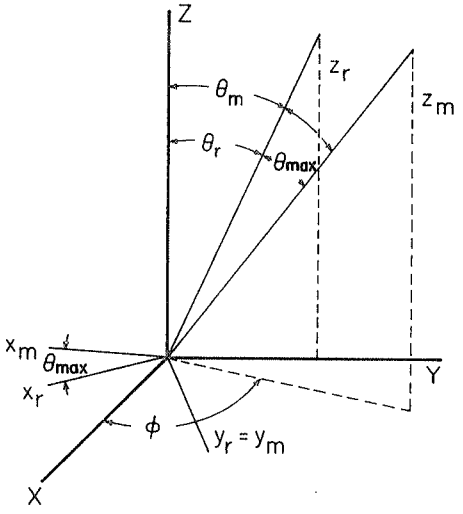

FIG. 4. The space-fixed XYZ, molecular $x_m y_m z_m$, and recoil $x_r y_r z_r$ coordinate frames. The molecule-fixed system has z_m along the molecular axis, and the recoil coordinate system has z_r along the asymptote of the separating fragments.

the other two Euler angles specifying the orientation of g_r with respect to g_m vanish. Then the direction cosines relating

the g_r and g_m coordinates take the particularly simple form,

$$\Phi_{g_r g_m} = \begin{pmatrix} \cos\theta_{max} & 0 & \sin\theta_{max} \\ 0 & 1 & 0 \\ -\sin\theta_{max} & 0 & \cos\theta_{max} \end{pmatrix} \tag{20}$$

namely, a counterclockwise rotation by θ_{max} about y_r (the line of nodes) brings g_m into coincidence with g_r. The angles of the g_m coordinate system with respect to the space-fixed coordinate system F are $\theta = \theta_r$, $\varphi = \varphi_r = \varphi_m$, and $\psi = \psi_r = \psi_m$. The direction cosine elements Φ_{Fg_m} that appear in Eq. (6) are transformed into linear combinations of the Φ_{Fg_r} by this axis rotation, so that

$$\begin{aligned} \Phi_{Fx_m} &= \cos\theta_{max}\,\Phi_{Fx_r} + \sin\theta_{max}\,\Phi_{Fz_r} \\ \Phi_{Fy_m} &= \Phi_{Fy_r} \\ \Phi_{Fz_m} &= -\sin\theta_{max}\,\Phi_{Fx_r} + \cos\theta_{max}\,\Phi_{Fz_r} \end{aligned} \tag{21}$$

The calculation of the fragment angular distribution now proceeds as before and simply "mixes" the previous results for axial (A) and transverse (T) recoil according to the expression

$$\begin{aligned} I(\theta) &= \cos^2\theta_{max}\, I_A(\theta) + \sin^2\theta_{max}\, I_T(\theta) \\ &= 1 + [I_A(\theta) - 1]\, P_2(\cos\theta_{max}) \end{aligned} \tag{22}$$

Equation (22) holds for a fixed value of θ_{max}. To obtain the actual angular distribution we must integrate over all θ_{max} weighting each value of θ_{max} by the normalized probability of finding the recoil angle in the range θ_{max} to $\theta_{max} + d\theta_{max}$, denoted by $P_{v,L}(\theta_{max})$, and then

we must sum over all rotational levels L and vibrational levels v that contribute to the photodissociation process

$$\overline{\overline{I(\theta)}} = \sum_{v} \sum_{L} \int_{0}^{2\pi} [\cos^2 \theta_{max} I_A(\theta) + \sin^2 \theta_{max} I_T(\theta)] P_{v,L}(\theta_{max}) d\theta_{max} \tag{23}$$

The distribution in θ_{max} will be determined by the transition probability for photodissociation at each internuclear separation r_c in each vibration-rotation level (v,L). This in turn depends on the shape of the potential curves for the ground and excited states, the thermal distribution of initial rotational and vibrational energy, and the spectral distribution of the pumping light.

Fortunately, the lowest vibrational levels of the ground state usually lie under a strongly sloping portion of the repulsive potential curve of the upper state. Then $V(r_c) - V(\infty) \gg L^2/2\mu r_c^2$, and direct trajectory calculations [2] show that θ_{max} deviates very little from $\theta_{max} = 0°$ (axial recoil) so that $\overline{\overline{I(\theta)}} \simeq I_A(\theta)$. Thus, the rotational blurring is normally quite small and the photofragment distribution corresponds closely to the "axial-recoil" limit.

Another way of regarding this problem is to view the rotational period of the molecule as an "internal clock" which measures the time the recoiling fragments spend close to each other. As the fragments separate their "moment arm" about the center of mass rapidly increases and the angle through which they rotate (in order to conserve angular momentum) decreases (see Fig. 3). Thus, the recoil angle θ_{max} is largely determined by the separation time of the fragments. The rotational period of molecules is typically on the order of 10^{-10}-10^{-11} sec, whereas the vibrational period is on the order of 10^{-12}-10^{-13} sec. If the molecule dissociates by a simple vibrational motion along the ruptured bond direction, the fragments will rotate typically about 5° as they dissociate and the "rotational blurring" of the photofragment angular distribution will be minimal. On the other hand, pronounced rotational blurring of the angular distribution permits an estimate to be made of the number of picoseconds required to rupture the chemical bond in the photodissociative process [8].

QUANTUM TREATMENT

The semiclassical treatment is not thoroughly satisfactory; for example, in contradiction to the uncertainty principle, both the

position $r = r_c$ and the momentum $p = 0$ must be specified at time $t = 0$ in order to calculate the recoil angle θ_{max} of the separating fragments. A quantum treatment has the advantage of considering simultaneously the radial and angular motions of the fragments so that the synthesis of the photofragment distribution from the axial and transverse recoil limits occurs in a natural manner. Moreover, a study of the correspondence between the quantum and classical treatments brings out more fully the conditions under which the axial-recoil approximation is valid.

The Differential Cross Section

In a quantum treatment the differential cross section (Θ, Φ) is proportional to the square of the transition dipole matrix element

$$I(\Theta, \Phi) \sim |\langle \psi_f | \mu \cdot \epsilon | \psi_i \rangle|^2 \tag{24}$$

where (Θ, Φ) are polar angles referred to the laboratory coordinate system. Let us concentrate our attention on a $^1\Sigma \rightarrow {}^1\Sigma$ or a $^1\Sigma \rightarrow {}^1\Pi$ dissociative transition caused by a beam of plane polarized light. For the bound state, the wave function may be written according to the Born-Oppenheimer separation as a product wave function

$$\begin{aligned} |\psi_i\rangle &= F_i(q_i, r)\, R_{vJ}(r)\, Y_{JM}(\theta,\varphi) \\ &= F_i(q_i,r)\, R_{vJ}(r) \left(\frac{2J+1}{4\pi}\right)^{\frac{1}{2}} D^J_{M0}(\varphi,\theta,0) \end{aligned} \tag{25}$$

Here, $F_i(q_i,r)$ is an electronic part which is a function of the electronic coordinates q_i and depends parametrically on the internuclear distance r, $R_{vJ}(r)$ is the vibrational part which satisfies the radial Schrödinger equation

$$\left[-\frac{1}{2\mu r^2}\frac{d}{dr}\left(r^2\frac{d}{dr}\right) + V(r) + \frac{J(J+1)}{2\mu r^2}\right] R_{vJ}(r) = E_{vJ} R_{vJ}(r) \tag{26}$$

for the potential function $V(r)$, and $Y_{JM}(\theta,\varphi) \propto D^J_{M0}(\varphi,\theta,0)$ is a rotational part which expressed the orientation of the molecule,

where the angles (θ,φ) refer to the polarization vector ϵ chosen as the axis of quantization and $D^{J}_{MM'}$ is a Wigner rotation matrix [14]. Equation (25) corresponds to a stationary state (v,J) of the molecule with definite values of the energy E_{vJ} and the angular momentum $J(J+1)$ of which the latter makes a projection M on the space-fixed Z axis (chosen to lie along ϵ) and a projection 0 on the molecule-fixed z axis (chosen to lie along the internuclear axis).

In a similar manner the repulsive state may also be factored into an electronic part and a nuclear part

$$\langle | \psi_q | = F_q^*(q_i,r)\, R_q^*(r) \tag{27}$$

However, the continuum nuclear wave function $R_q^*(r)$ must be chosen to satisfy the proper boundary conditions for scattering, namely, that $R_q^*(r)$ has the asymptotic form of a plane wave plus an incoming spherical wave

$$R_q^*(r) \xrightarrow[r\to\infty]{} A[\exp(i\kappa \cdot r) + f(\theta)\exp(-i\kappa r)/r] \tag{28}$$

where κ is the propagation vector and r is the position vector. Here κ points along the final recoil direction of the fragments and r coincides with the molecular axis, as pictured in Fig. 5. Then the final state wave function for a repulsive $^1\Sigma$ state may be put into a form similar to Eq. (25):

$$\begin{aligned}\langle \psi_f (^1\Sigma) | &= F_q^*(q_i,r)\Sigma_{J'}\,(2J'+1)\,(i)^{J'}\exp(-i\delta_{J'})\,R_{J'}(\kappa r)\,P_{J'}(\hat{\kappa}\cdot\hat{r}) \\ &= F_q^*(q_i,r)\Sigma_{J'}\,(2J'+1)\,(i)^{J'}\exp(-i\delta_{J'})\,R_{J'}(\kappa r)\,D^{J'}_{00}(\hat{\kappa}\cdot\hat{r})\end{aligned} \tag{29}$$

where R_J satisfies Eq. (26) for the repulsive upper state potential and has the form at large internuclear separation of a sine wave, $\sin(\kappa r - \frac{1}{2}J'\pi + \delta_{J'})/\kappa r$ where $\delta_{J'}$ is the phase shift. For a repulsive $^1\Pi$ state, Eq. (29) must be modified to express the fact that the total angular momentum J makes a projection of one unit upon the internuclear axis $\hat{r}$ and the recoil axis $\hat{\kappa}$:

$$\langle \psi_q (^1\Pi) | = F_q^*(q_i,r)\,\Sigma_{J'}(2J'+1)\,(i)^{J'}\exp(-i\delta_{J'})\,R_{J'}(\kappa r)\,D^{J'}_{11}(\hat{\kappa}\cdot\hat{r}) \tag{30}$$

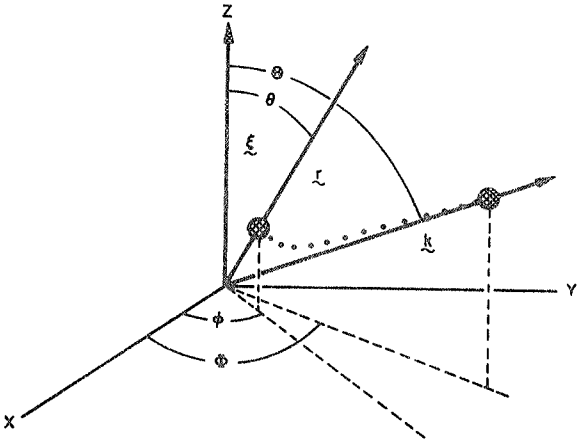

FIG. 5. The recoiling fragment (whose classical trajectory is indicated by the dotted line) is scattered by the repulsive molecular potential. The quantization axis ϵ is along the Z axis; the propagation vector κ is along the asymptote of the recoiling fragments; and the position vector r coincides with the molecular axis. For molecular dissociation the recoiling fragments generally have considerable kinetic energy so that κ is nearly parallel to r.

The angles in Eqs. (29) and (30) are measured between the unit vectors κ and r, and they are not the same angles as in Eq. (25). However, they may be related to the angles (θ, φ) and (Θ, Φ) by the successive application of two rotations (see Fig. 5). In general, if the rotation $(\alpha\beta\gamma)$ results from the rotation $(\alpha_1\beta_1\gamma_1)$ followed by the rotation $(\alpha_2\beta_2\gamma_2)$ then

$$D^j_{m'm}(\alpha\beta\gamma) = \Sigma_{m''} D^j_{m'm''}(\alpha_2\beta_2\gamma_2) D^j_{m''m}(\alpha_1\beta_1\gamma_1) \qquad (31)$$

Equation (31) is a generalization of the spherical harmonic addition theorem [14] which may be obtained by setting $m' = m = 0$. Applying Eq. (31) to Eqs. (29) and (30) and using the fact that

$$D^{j*}_{m'm}(\alpha\beta\gamma) = D^j_{m'm}(-\alpha\beta-\gamma) \qquad (32)$$

we obtain for the final state wave function the expression

$$\langle \psi_q | = \Sigma_{J'M'} (2J'+1)(i)^{J'} \exp(-i\delta_{J'}) R_{J'}(\kappa r)$$

$$D^{J'*}_{M'\Lambda}(\varphi,\theta,0)\, D^{J'}_{M'\Lambda}(\Phi,\Theta,0) \qquad (33)$$

where for a $^1\Sigma$ state $\Lambda = 0$ while for a $^1\Pi$ state $\Lambda = 1$. The final state wave function given by Eq. (31) corresponds to a stationary state of the molecule with a definite value of the energy $E = \kappa^2/2\mu$, but not to a definite state of angular momentum although the projection of the latter along r and κ is well defined [15].

The interaction term $\mu \cdot \epsilon$ appearing in Eq. (24) may also be expressed in terms of the angles defined in Fig. 5. For a $^1\Sigma - {}^1\Sigma$ transition (parallel-type transition) the angular part of $\mu \cdot \epsilon$ transforms as $\Phi_{Zz}(\varphi,\theta,0) = D^1_{00}(\varphi,\theta,0)$ whereas for a $^1\Sigma - {}^1\Pi$ transition (perpendicular-type transition) the angular part of $\mu \cdot \epsilon$ transforms as $\Phi_{Zx}(\varphi,\theta,0)$ and $\Phi_{Zy}(\varphi,\theta,0)$, which are related to $D^1_{01}(\varphi,\theta,0)$. Upon replacing in Eq. (24) $|\psi_i\rangle$ by Eq. (25), $\langle \psi_q |$ by Eq. (33) and $\mu \cdot \epsilon$ by the above, the differential cross section may be put into the form [2]

$$I(\Theta,\Phi) \sim |\Sigma_{J'}\Sigma_{M'}\mathcal{R}_{J'}\mathcal{A}_{J'} D_{M'\Lambda}(\Phi,\Theta,0)|^2 \qquad (34)$$

where

$$\mathcal{R}_{J'} = (i)^{J'} \exp(-i\delta_{J'}) \int R_{vJ}(r)\, \mathcal{M}(r)\, R_{J'}(\kappa r) r^2 dr \qquad (35)$$

is a radial term governing the band strength of the transition which depends upon the electronic transition dipole moment

$$\mathcal{M}(r) = \int F_q^*(q_i,r)\, \Sigma_i e\, q_i\, F_i(q_i,r)\, dq_i \qquad (36)$$

and

$$\mathcal{A}_{J'} = (2J'+1)\left[\int D^{J'*}_{M'\Lambda}\, D^1_{0\lambda}\, D^J_{M0}\, d\Omega\right] D^{J'}_{M'\Omega}(\Phi,\Theta,0)$$

$$= C(J1J';M0)\, C(J1J';0\lambda)\, D^{J'}_{M'\Lambda}(\Phi,\Theta,0) \qquad (37)$$

is an angular term giving in terms of Clebsch-Gordon coefficients the rotational line strength for a specific $JM \rightarrow J'M'$ transition.

Equation (34) is the photofragment angular distribution arising from one (J,M) sublevel. It is quite complex in form and is no longer of the dipolar form given by Eq. (13). However, if the molecular ensemble is randomly oriented and has equal M state populations, then the photofragment angular distribution is obtained from Eq. (34) by summing over all the M sublevels of the initial state:

$$I(\Theta,\Phi) = \Sigma_M \left| \Sigma_{J'} \Sigma_{M'} \mathcal{R}_{J'} \, C(JlJ';M0)\, C(JlJ';0\lambda) D^{J'}_{M'\Omega}(\Phi,\Theta,0) \right|^2 \tag{38}$$

where we omit all factors that do not affect the form of the angular distribution. By substituting explicit algebraic expressions for the Clebsch-Gordan coefficients in Eq. (38), $I(\Theta, \Phi)$ may now be shown [2] to have the form $[1 + \beta P_2 (\cos \Theta)]/4\pi$. In particular, for a parallel-type transition

$$\beta_{\parallel} = \frac{J(J-1)|\mathcal{R}_{J-1}|^2 + (J+1)(J+2)|\mathcal{R}_{J+1}|^2 - 3J(J+1)(\mathcal{R}^*_{J+1}\mathcal{R}_{J-1} + \mathcal{R}_{J+1}\mathcal{R}^*_{J-1})}{(2J+1)[J|\mathcal{R}_{J-1}|^2 + (J+1)|\mathcal{R}_{J+1}|^2]} \tag{39}$$

Note that in the limit $|\mathcal{R}_{J-1}| = |\mathcal{R}_{J+1}|$, $\beta_{\parallel} = 2$.

The Axial-Recoil Approximation

The actual evaluation of the photofragment distribution, given by Eq. (38), requires a knowledge of the variation of the radial terms $\mathcal{R}_{J'}$ with J' over the limited range $\Delta J' = 0, \pm 1$ permitted by the dipole selection rules. We are interested in the common situation where the kinetic energy of the fragments is much larger than the rotational energy (on the order of kT) of the parent molecule. In this case the phase shift $\delta_{J'}$ appearing in Eq. (35) may be estimated to good approximation from the WKB expression [16]

$$\delta_{J'} = \frac{\pi}{2}(J+\tfrac{1}{2}) - \kappa r_c + \int_{r_c}^{\infty} \kappa\{1-[(J'+\tfrac{1}{2})/\kappa r]^2\}^{\frac{1}{2}} dr - \int_{r_c}^{\infty} k\,dr \tag{40}$$

where $\kappa^2 = 2\mu[E-V(r)]$ and $k^2 = 2\mu E$. By expanding the expression within the braces "{ }" in Eq. (40), we find that

$$\delta_{J'} = \frac{\pi}{2} J' - C \tag{41}$$

where C is a constant to order $[(J' + \frac{1}{2})/\kappa r]^2$. To this approximation, the factor $(i)^{J'} \exp(-i\delta_{J'})$ appearing in Eq. (35) equals $\exp(iC)$ and is independent of J'. Furthermore, under these conditions the form of the radial continuum wave function $R_{J'}(r)$ is almost exclusively determined by the shape of the repulsive potential term $V(r)$ rather than the centrifugal potential term $J'(J'+1)/2\mu r^2$ appearing in Eq. (26). Consequently, when $\kappa r \gg J' + \frac{1}{2}$

$$\mathcal{R}_{J+1}(r) \simeq \mathcal{R}_{J-1}(r) \tag{42}$$

Consequently, the radial term $\mathcal{R}_{J'}$ is effectively a constant over the rotational structure and may be taken outside the sum over J' and M' appearing in Eq. (38).

With this approximation, the sums over J', M', and M are readily performed with the help of the identities [14]

$$\Sigma_{J'} \Sigma_{M'} C(J1J';M0)\, C(J1J';0\lambda) D^{J'}_{M'\lambda}(\Phi,\Theta,0)$$

$$= D^{J}_{M0}(\Phi,\Theta,0)\, D^{1}_{0\lambda}(\Phi,\Theta,0) \tag{43}$$

and

$$\Sigma_M |D^J_{M0}|^2 = 1 \tag{44}$$

The photofragment angular distribution reduces to

$$I(\Theta,\Phi) = |D^1_{0\lambda}(\Phi,\Theta,0)|^2 \tag{45}$$

i.e., for a $^1\Sigma$-$^1\Sigma$ transition ($\lambda = 0$), $I(\Theta,\Phi)$ is proportional to $\cos^2\Theta$, whereas for a $^1\Sigma$-$^1\Pi$ transition ($\lambda = 1$), $I(\Theta,\Phi)$ is proportional to $\sin^2\Theta$. These are exactly the results we obtained previously in the case of axial recoil (see Table 2). Hence, the validity of the axial recoil approximation rests on the extent to which $\mathcal{R}_{J+1} = \mathcal{R}_{J-1}$, which in turn depends on the extent to which $\delta_{J+1} - \delta_{J-1} = \pi$. As

κr grows in magnitude compared to $(J' + \frac{1}{2})$ the axial-recoil approximation is expected to describe the photoejection dynamics with increasing accuracy. However, close to threshold, the axial-recoil angular distribution is "blurred" by the rotational motion of the molecule and we must compute quantum mechanically the interference between the $(J + 1)$ and $(J - 1)$ outgoing spherical waves.

In molecular photodissociation the fragments are so heavy that their motion is essentially classical. However, if one of the fragments is an electron, it is not surprising to find that a fully quantum treatment is required to account for the angular distribution of the photoejected electrons. For example, Cooper and Zare have used Eq. (39) to calculate the form of the angular distribution of the photoelectrons and they have applied with considerable success their calculations to the recent laser photodetachment measurements of Hall and co-workers [17] at the University of Colorado. Note, however, that this simple treatment neglects magnetic forces (spin-orbit effects) which can be important in determining the form of the photoelectron anisotropy [18].

APPLICATIONS

The first attempts to observe a possible anisotropy in the angular distribution of photodissociation products was the study of the NaI photodissociation process

$$NaI + h\nu \rightarrow Na^* + I \qquad (46)$$

by Mitchell [19], and later by Hanson [20]. They measured the Doppler width of the resulting sodium D emission lines as a function of angle, but they found no observable difference when the atomic fluorescence was viewed parallel or perpendicular to the incident light beam. This finding, although disappointing, is not incompatible with the treatment outlined in the last two sections. It appears that more than one repulsive state contributes to the NaI photodissociation process, and that these repulsive states are a mixture of parallel and perpendicular characters. Consequently, the expected anisotropy is greatly reduced, if not effectively "washed out" [21].

Ironically, the first successful observations of angular anisotropies were not through photodissociation studies but through studies of the more complex phenomena of electron impact dissociation [22]. Recently, there have been several strikingly

successful studies of angular anisotropies produced by electron impact, in particular the dissociative ionization of H_2 and other molecules [23], the production of energetic metastables in the electron impact dissociation of H_2 [24], the observation of polarized emission from the excited atomic fragments resulting from the impact breakup of H_2 [25], and the angular distribution of O^- from the dissociative attachment of electrons to O_2 [26]. In addition, dissociation by heavy particle impact should also be expected to yield anisotropic fragment distributions, and this has been borne out in several recent experimental studies of molecular dissociation by fast ion and neutral particle beams impinging on target molecules [27].

In the preceding sections a fairly general treatment of photoejection dynamics has been presented. We consider here the application of these principles to two current photochemical experiments: "photolysis mapping" by Bersohn and co-workers at Columbia University [7] and "photofragment spectroscopy" by Wilson and co-workers at the University of California at San Diego [8]. Both exploit information about the anisotropic photofragment distribution to learn about the nature of the dissociative state.

Photolysis Mapping

The first successful demonstration of the existence of anisotropies in the angular distribution of photofragments was the work of Solomon [7], who irradiated a hemispherical or a rectangular cell containing gas at low pressure with a beam of light. The inner walls of the container are coated with a thin layer of a metallic film (a metallic mirror). The angular dependence of the photofragments is detected by the differential rate of removal of the metallic mirror by the reactive fragments, in the classical manner that Paneth and Hofeditz [28] first detected the presence of free radicals. The disappearance of the metallic film is caused by the reaction of the metal atoms with the photofragments to form volatile metal compounds that may be pumped away. Alternatively, for that small class of compounds that are volatile but whose fragments are nonvolatile, the photolysis of the volatile compounds yields directly a deposit of the nonvolatile photofragment on the walls of the container. In either case, the photofragment angular distribution "maps itself" onto the walls of the hemispherical or rectangular vessel. Figure 6 shows a schematic diagram of this simple "bulb" experiment.

The technique of photolysis mapping has been used so far to

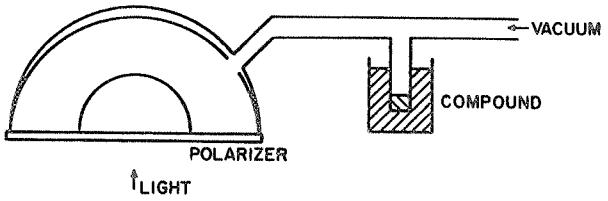

FIG. 6. Schematic diagram of photolysis mapping apparatus. The compound to be photolyzed is placed in a thermostatted bath to control its vapor pressure. The light from a 1000-W xenon-mercury dc arc source is incident upon the face of the hemisphere which is a front quartz plate. The light may be linearly polarized by inserting a UV transmitting polarizer in front of the quartz plate. From Jonah et al. [7].

FIG. 7. Hemisphere in which cadmium has been deposited during photolysis of $Cd(CH_3)_2$ using unpolarized light directed perpendicular to the plane of this figure. The bright spots are reflections of the flashbulb used in making this photograph. From Jonah et al. [7].

measure the anisotropic distributions resulting from the photodissociation of Br_2,I_2, formaldehyde, acetaldehyde, proprionaldehyde, acetone, and cadmium dimethyl [7]. Perhaps the most striking effect is achieved with the last-named compound, $Cd(CH_3)_2$. Figure 7 shows a glass hemisphere, 2 in. in diameter, inside of which cadmium dimethyl has been photolyzed for 9 hr by unpolarized light of a 1000-W xenon-mercury dc arc source directed against the flat face (quartz plate) of the hemisphere (see Fig. 6) with uniform intensity across its surface. The deposition of cadmium is distributed more or less isotropically in the direction of the light beam but evidently is mainly at the pole and in streaks. This deposition pattern is caused by the fact that the sticking coefficient of cadmium atoms on a cadmium surface is several orders of magnitude greater than on a glass surface. Figure 8 shows the results of a similar experiment in which plane polarized light is

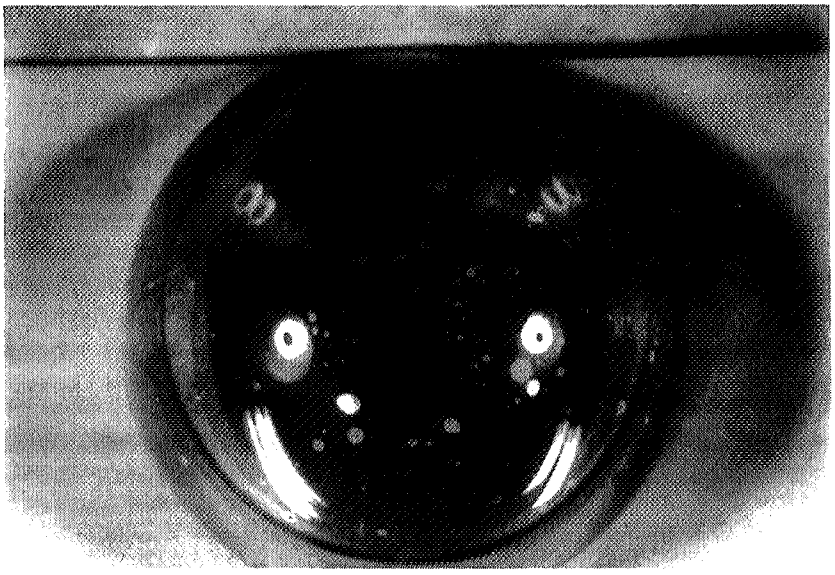

FIG. 8. Hemisphere in which cadmium has been deposited during photolysis of $Cd(CH_3)_2$ using linearly polarized light. The light beam is directed perpendicular to the plane of this figure with its polarization vector in the vertical plane. The bright spots are reflections of the flashbulb used in making this photograph. From Jonah et al. [7].

used by placing a polarizer against the face of the hemisphere (see Fig. 6). The cadmium atom distribution is more anisotropic in form, peaking in the direction of the light beam but at right angles to the direction of the electric vector. Figure 7 and 8 correspond to projections of Figs. 2c and 2d onto a hemispherical surface. Figures 7 and 8 show that the transition moment is essentially perpendicular to the motion of the cadmium atoms.

It is also possible to detect the methyl radical distribution by coating the inside walls with molybdenum trioxide, a white powder which turns blue when it reacts with methyl radicals. A rectangular box was prepared from microscope slides that had been exposed to "smoke" generated by placing a molybdenum wire in the flame of a Bunsen burner. Figure 9 shows the microscope slides following photolysis of $Cd(CH_3)_2$ by plane polarized light. The two darker

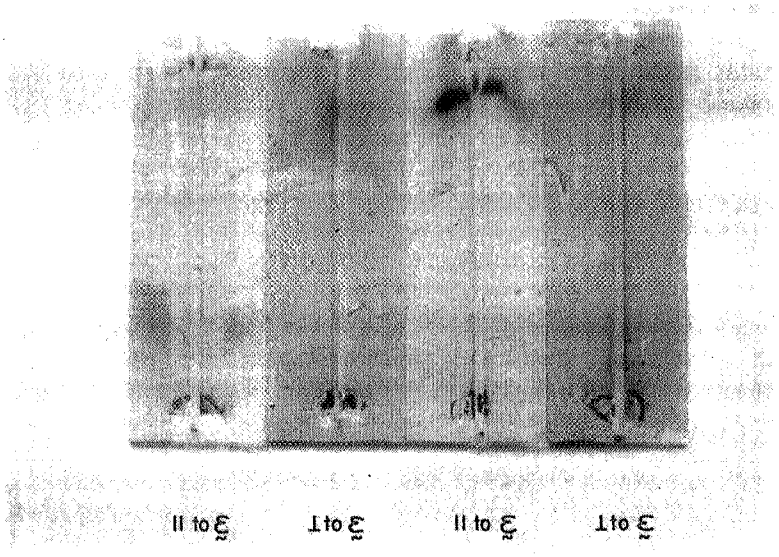

FIG. 9. The appearance of four microscope slides coated with MoO_3 forming the walls of a rectangular cell in which $Cd(CH_3)_2$ was photolyzed. The darker slides were perpendicular to the polarization vector ϵ of the light beam; the lighter ones were parallel. In the middle of each slide is a small capillary tube that is used to collect for ESR studies the blue Mo(v) compound resulting from the reaction of the white MoO_3 coating with CH_3 radicals. From Jonah et al. [7].

(bluer) slides were the ones positioned perpendicular to the electric vector of the polarized light while the two lighter (whiter) slides were parallel. Thus the CH_3 photofragments are found to exhibit the same angular distribution as the cadmium atoms.

Together, Figs. 7, 8, and 9 offer dramatic visual proof for the existence of angular anisotropies in the photofragment distribution. From these measurements, Bersohn and co-workers [7] conclude that the "linear" molecule $Cd(CH_3)_2$ photodissociates in the near UV by a perpendicular-type transition, and because both the cadmium and methyl radicals separate in a direction perpendicular to the transition moment, the fragments likely exit along a ruptured $Cd-CH_3$ bond axis through an antisymmetric stretching vibration. This vibration leaves one $Cd-CH_3$ bond overextended (which breaks) while the other $Cd-CH_3$ bond is highly compressed. Bersohn and co-workers then propose that a second CH_3 radical departs about half a vibrational period later than the first. This successive fragmentation process is energetically allowed and is in accord with a molecular orbital analysis of this weakly allowed metal alkyl transition in which the perpendicular transition moment is attributed to vibronic perturbation of the excited states by the low frequency bending vibrations.

The photolysis mapping technique is unquestionably highly ingenious and remarkably simple. However, its surface detection scheme suffers from the vagaries associated with the study of other surface phenomena, namely, problems of surface preparation, surface history, and surface contamination severely limit the reproducibility of the results. Consequently, it is quite difficult to achieve accurate quantitative measurements of the angular anisotropy by these "bulb" experiments. A most promising alternative is the "beam" experiments of Wilson et al. [8] which unfortunately require a much more ambitious investment in instrumentation.

Photofragment Spectroscopy

Figure 10 illustrates the apparatus for photofragment spectroscopy. A beam of molecules is crossed with a pulsed beam of polarized light from a laser. Those photodissociation fragments that recoil at a laboratory angle Θ, measured from the electric vector of the light beam, are detected by a quadrupole mass spectrometer located a known distance away from the intersection region of the two beams. The fragment distribution as a function of mass, of time, and of laboratory angle Θ, is determined for each laser photon energy (wavelength). The entire experiment has been automated and is run under the control of a computer

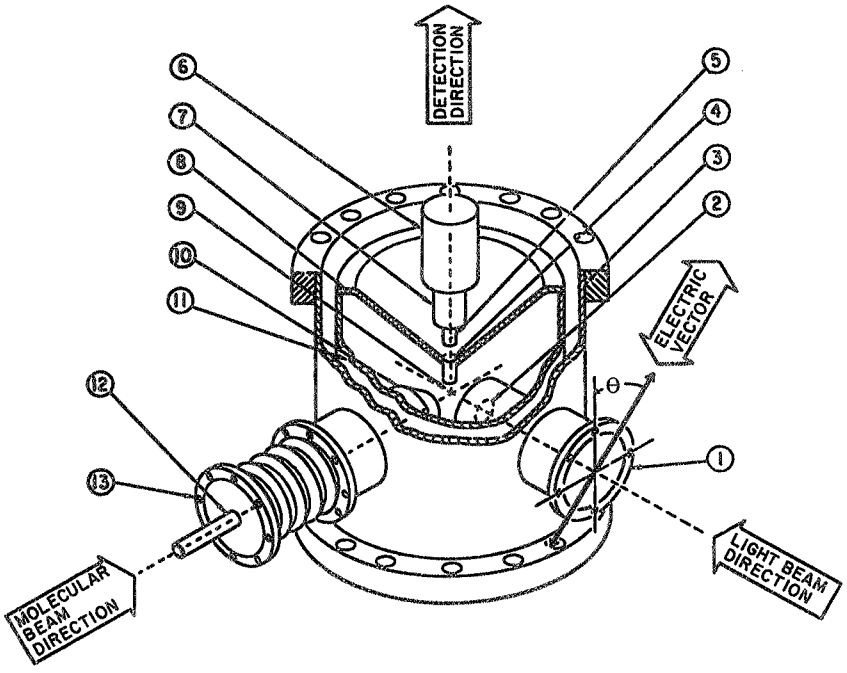

FIG. 10. Cutaway drawing of photofragment spectrometer. The beam of molecules enters from the left where it crosses at right angles a pulsed beam of polarized light from a laser. Those photofragments that recoil upward are detected by a quadrupole mass spectrometer as a function of mass, photon energy, flight time, and direction of recoil, Θ, measured from the electric vector of the light beam. The interaction region and mass spectrometer are in separately pumped chambers connected by a liquid-nitrogen-cooled tube that serves to collimate the fragments. The numbered components are: (1) laser beam port, (2) lens to match diameter of laser beam to that of molecular beam, (3) outer walls of bakable ultra-high-vacuum chamber, (4) liquid-nitrogen-cooled collimating tube, (5) mass spectrometer electron bombardment ionizer, (6) mass spectrometer electron multiplier, (7) quadrupole mass spectrometer,

(8) liquid-nitrogen-cooled partition between interaction and detection chambers, (9) interaction volume, (10) liquid-nitrogen-cooled molecular beam collimator, (11) liquid-nitrogen-cooled inner wall of interaction chamber, (12) molecular beam oven with capillary slits, and (13) molecular beam port. From Busch, Cornelius, Mahoney, Morse, Schlosser, and Wilson [8].

which rotates the half-wave plate to give a chosen value of Θ, fires the pulsed laser, collects the electron multiplier output of the quadrupole mass filter, and averages it over many cycles.

From the variation of the photofragment signal with Θ, the angular distribution of fragment recoil with respect to the polarization is determined; from the variation of the time-of-flight delay between the laser pulse and the photofragment signal, the translational velocity of the fragment of known mass, and hence the fragment translational energy, is determined. According to the conservation of energy,

$$E_{\text{parent}} + h\nu_{\text{laser}} = D + E_{\text{internal}} + E_{\text{translational}} \tag{47}$$

where the thermal energy of the parent molecule plus the laser photon energy is equated to the internal and translational energy of the fragments plus the energy required to dissociate the parent molecule into the observed fragments. The distribution of E_{parent} is readily estimated from a knowledge of the molecular beam oven temperature, and the value of D is usually available for the more common molecules. Hence, a measurement of $E_{\text{translational}}$ permits as well a determination of the internal energy states of the fragments. Using the ultra-high-vacuum beam machine shown in Fig. 10, Wilson and co-workers have investigated one or more photodissociative transitions in Cl_2, Br_2, IBr, I_2, ICN, NO_2, NOCl, several alkyl iodides, and ethyl nitrite [8].

Perhaps the power of the photofragment spectroscopy technique is best illustrated by reviewing their recent work on the photodissociation of the I_2 molecule. The well-known I_2 absorption spectrum consists of a banded structure in the visible above 5000 Å, which at shorter wavelengths merges into a continuum. This has been traditionally interpreted, ever since the celebrated work of Franck [29], as corresponding to a series of transitions from the $v'' = 0$ level of the ground state to high v' levels of an excited electronic state, even reaching to unquantized radial motion at higher

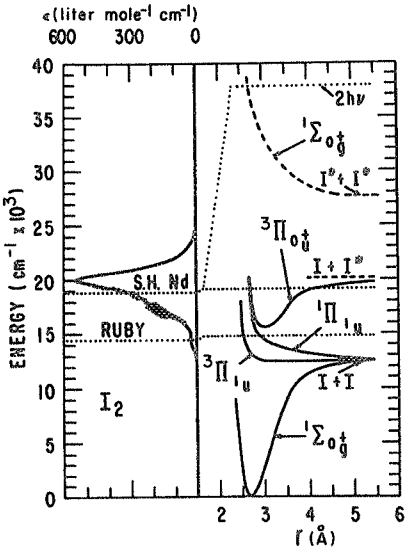

FIG. 11. The I_2 absorption spectrum and potential curves. Irradiation with the ruby laser fundamental at 14,405 cm^{-1} gives the results shown in Fig. 12. Irradiation with the neodymium laser second harmonic at 18,830 cm^{-1} or with the output of a laser-pumped dye laser in the same wavelength region gives iodine atoms which probably arise from at least three sources: (1) both iodine atoms are unexcited and presumably arise from the $^1\Pi_{1u}$ state (see Fig. 14, upper panel); (2) one iodine atom is excited and the other is unexcited corresponding to dissociation from the $B\,^3\Pi_{0^+u}$ state (see Fig. 14, lower panel); and (3) both iodine atoms are excited, which is attributed to sequential or simultaneous absorption of two photons to reach a repulsive $^1\Sigma_g^+$ final state. From Wilson [8].

energies than the dissociation limit of this excited state. Figure 11 shows the I_2 absorption spectrum and potential curves of the known electronic states of I_2. The assignments are from Mulliken [30], and Mathieson and Rees [31].

In their first experiments, Wilson and co-workers irradiated I_2 with the red light (14,405 cm^{-1}) from a pulsed ruby laser which coincides with the weak absorption continuum shown in Fig. 11. They found, from the time-of-flight of the iodine atoms, illustrated in Fig. 12, that the iodine atoms are produced exclusively in their ground electronic states, the only energetically allowed states for a one-photon process. Moreover, they found, as illustrated in Fig. 13, that the angular distribution peaked at about 90° to the

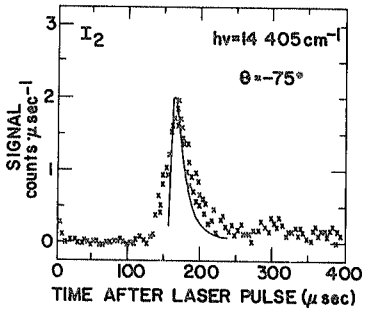

FIG. 12. Time-of-flight spectrum of the iodine fragments resulting from the photodissociation of I_2 by ruby laser light at 14,405 cm^{-1}. From Wilson [8].

electric vector of the light beam. Hence, the photodissociation of I_2 at this long wavelength corresponds to a perpendicular transition, and the results are consistent with dissociation from the upper $^3\Pi_{1u}$ or $^1\Pi_{1u}$ states.

In their second experimental study of the photodissociation of I_2, Wilson and co-workers crossed an I_2 beam with pulses of polarized light from a laser-pumped dye laser tuned to wavelengths around the peak of the absorption continuum shown in Fig. 11. The mass filter signal at two different values of the angle Θ are presented in Fig. 14. The upper panel corresponds approximately to a measurement perpendicular to the electric vector while the lower panel corresponds to a measurement nearly parallel to the electric vector. We see that two distinct time-of-flight peaks appear: the shorter one observed at $\Theta = -70°$ corresponds to the two iodine atoms in their ground state; the longer one observed at $\Theta = +20°$ corresponds to one iodine atom unexcited ($^2P_{\frac{3}{2}}$) and one

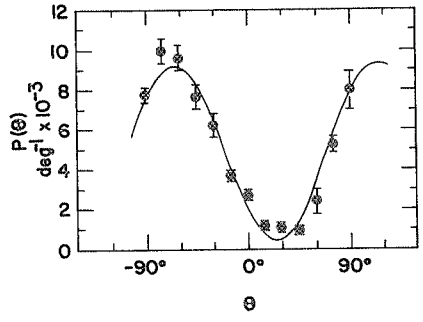

FIG. 13. Angular distribution of the photofragment spectrum of I_2 photodissociated by ruby laser light at 14,405 cm^{-1}. The solid curve is a least-square fit of $a + b \sin^2 (\Theta - \Theta_0)$ to the data. From Wilson [8].

iodine atom excited ($^2P_{\frac{1}{2}}$). Thus, Wilson and co-workers have demonstrated that the long accepted assignment [28-30] of the main I_2 visible continuum as originating almost exclusively from a transition to the $B^3\Pi_{0^+u}$ state is incorrect; instead, the photodissociation of I_2 occurs from more than one repulsive state which together have a mixture of parallel and perpendicular character. Similar measurements have been carried out at other photon energies and the ratio of $0_g \rightarrow 1_u$ (perpendicular) $0_g \rightarrow 0_u$ (parallel) transition probabilities for this Hund's case (c) molecule are 1.2 ± 0.2 at 20,850 cm^{-1}, 1.3 ± 0.1 at 21,510 cm^{-1}, and 2.3 ± 0.5 at 22,230 cm^{-1}. These measurements are consistent with earlier photolysis mapping experiments which showed a predominantly perpendicular angular distribution for the recoiling atoms. However, the photofragment spectroscopy studies of Wilson et al. clearly resolve the continuum absorption into its separate parallel ($^3\Pi_{0^+u}$) and perpendicular (presumably $^1\Pi_{1u}$) components. Thus, one of the most studied of molecular spectra once again reveals hidden wrinkles, as uncovered by this new photochemical technique. This forces us to rethink anew past experiments involving I_2 continuum oscillator strengths, iodine atom quenching, and iodine atom reactions produced by the photolysis of I_2 in the visible.

The application of photofragment spectroscopic and photolysis

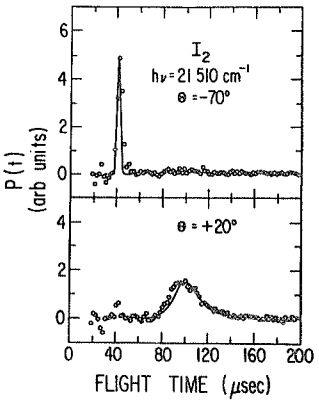

FIG. 14. Photofragment spectrum of I_2 photodissociated by 21,510 cm^{-1} light. The upper panel is a lu state dissociating into ground state atoms. The lower panel is a 0^+u state dissociating into one ground and one excited state atom. The angle Θ is the recoil angle of the fragments measured with respect to the electric vector of the light beam. The open circles are from the measured signals, averaged over 242 laser pulses. The solid lines are the calculated line shapes and positions normalized to the heights of the measured peaks. From Oldman et al. [8].

mapping to a study of the photodecomposition of simple nonlinear polyatomics promises to be even more informative as the first experiments on NO_2 [8], and on aliphatic carbonyls [7] have borne out.

CONCLUSIONS

A few concluding remarks perhaps are now in order. Modern photochemistry stands at a crossroads in its development. In the not too distant past photochemists concerned themselves almost exclusively with the bulk chemical changes that accompany the absorption of light. These macroscopic transformations were studied in the same manner as classical kinetics, requiring

fiendishly clever experiments in hopes of elucidating the important photochemical pathways. Certainly these types of experiments must continue. However, the photochemist now has at his command powerful new means to explore the microscopics of photochemistry, namely, the primary fragmentation step in a photochemical process. It is believed that a study of photoejection dynamics, or what might be called "the anatomy of a photochemical reaction" will lead the way to a deeper understanding of the nature of the photochemical pathways investigated by more traditional means.

ACKNOWLEDGMENTS

It is a pleasure to acknowledge the many contributions of Professor Dudley R. Herschbach who originally suggested the study of photoejection dynamics as a thesis topic and who patiently guided the author through the peaks and valleys of graduate research. Figures 6-14 are reproduced with the kind permission of their respective authors. The author also wishes to thank the organizing committee who invited him to participate in the Sixième Conférence Internationale de Photochimie. This work was supported, in part, by the National Science Foundation and by the Army Research Office, Durham.

REFERENCES

[1] Adapted from an invited talk presented at the Sixth International Conference of Photochemistry, Bordeaux, France, September 6-8, 1971.

[2] R. N. Zare, "Molecular Fluorescence and Photodissociation," thesis, Harvard Univ., Cambridge, Mass., 1964. See also R. N. Zare and D. R. Herschbach, Proc. I.E.E.E., 51, 173 (1963); R. N. Zare and D. R. Herschbach, "Mechanics of Molecular Photodissociation," Univ. of Calif. Lawrence Radiation Lab. Report UCRL-10438, 1963; "Proposed Molecular Beam Determination of Energy Partition in the Photodissociation of Polyatomic Molecules" UCRL-11359, 1964. R. N. Zare and D. R. Herschbach, Appl. Optics Chem. Lasers Suppl., 2, 193 (1965); R. N. Zare, J. Chem. Phys., 47, 204 (1967); J. Cooper and R. N. Zare, J. Chem. Phys., 48, 942 (1968); R. J. Van Brunt and R. N. Zare, J. Chem. Phys., 48, 4304 (1968); J. Cooper and R. N. Zare, Lectures in

Theoretical Physics XI-C (S. Geltman, K. T. Mahanthappa, and W. E. Brittin, eds.), Gordon and Breach, New York, 1969, pp. 317-337.

[3] E. U. Condon and G. H. Shortley, The Theory of Atomic Spectra, Cambridge Univ. Press, London and New York, 1935, p. 97.

[4] R. Bersohn and S. H. Lin, Advan. Chem. Phys., 16, 80 (1969).

[5] H. G. Dehmelt and K. B. Jefferts, Phys. Rev., 125, 1318 (1962); C. B. Richardson, K. B. Jefferts, and H. G. Dehmelt, Phys. Rev., 165, 80 (1968); K. B. Jefferts, Phys. Rev. Letters, 20, 39 (1968); 23, 1476 (1969).

[6] J. V. V. Kasper and G. C. Pimentel, Appl. Phys. Letters, 5, 231 (1964); M. A. Pollack, Appl. Phys. Letters, 9, 94 (1966); C. R. Guiliano and L. D. Hess, J. Appl. Phys. 40, 2428 (1969); J. D. Campbell and J. V. V. Kasper, Chem. Phys. Letters, 10, 436 (1971).

[7] J. Solomon, J. Chem. Phys., 47, 889 (1967); C. Jonah, P. Chandra, and R. Bersohn, J. Chem. Phys., 55, 1903 (1971); J. Solomon, C. Jonah, P. Chandra, and R. Bersohn, J. Chem. Phys., 55, 1908 (1971); C. Jonah, J. Chem. Phys., 55, 1915 (1971); see also S. Karplus, "Molecular Photodissociation Processes," thesis, Columbia Univ., New York, 1965).

[8] K. R. Wilson, Discussions Faraday Soc., 44, 234 (1967); G. E. Busch, R. T. Mahoney, and K. R. Wilson, I.E.E.E. Quantum Electron., QE-6, 171 (1970); K. R. Wilson, "Photofragment Spectroscopy of Dissociative Excited States," in Chemistry of the Excited State (J. N. Pitts, Jr., ed.), Gordon and Breach, New York, in press; G. E. Busch, R. T. Mahoney, R. I. Morse, and K. R. Wilson, J. Chem. Phys., 51, 449, 837 (1969); G. E. Busch, J. R. Cornelius, R. T. Mahoney, R. I. Morse, D. W. Schlosser, and K. R. Wilson, Rev. Sci. Instr., 41, 1066 (1970); R. J. Oldman, R. K. Sander, and K. R. Wilson, J. Chem. Phys., 54, 4127 (1971); G. E. Busch and K. R. Wilson "Triatomic Photofragment Spectra: I. Energy Partitioning in NO_2 Photodissociation," "II. Angular Distribution from NO_2 Photodissociation," and "III. NOCl Photodissociation," J. Chem. Phys., in press. For similar work see R. W. Diesen, J. C. Wahr, and S. E. Adler, J. Chem. Phys., 50, 3635 (1969); ibid., 55, 2812 (1971).

[9] E. U. Condon, Am. J. Phys., 15, 365 (1947).

[10] A. R. Edmonds, Angular Momentum in Quantum Mechanics, Princeton Univ. Press, Princeton, New Jersey, 1957, pp. 6-8.

[11] H. Sponer and E. Teller, Rev. Mod. Phys., 13, 76 (1941). Group theory considerations can only tell us which transitions

are allowed and which are forbidden for a certain orientation of the molecule with respect to the source of excitation. However, this information often suffices to place bounds on the shape of the angular distribution of the dissociation products. In the related case of dissociative electron impact G. H. Dunn [Phys. Rev. Letters, 8, 62 (1962)] has discussed the general form of the differential cross section determined by the symmetries of the initial and final molecular states.

[12] See R. A. Fox, R. M. Kogan, and E. J. Robinson, Phys. Rev. Letters, 26, 1416 (1971). For experimental studies of multiphoton molecular dissociation and/or ionization see N. K. Berezhetskaya, G. S. Voronov, G. A. Delone, N. B. Delone, and G. K. Piskova, Soviet Phys. JETP, 31, 403 (1970); P. Agostini, M. Lu Van, and G. Mainfray, Phys. Letters, 36A, 21 (1971); S. L. Chin, Phys. Rev., A4, 992 (1971).

[13] J. O. Hirschfelder, C. F. Curtiss, and R. B. Bird, Molecular Theory of Gases and Liquids, Wiley-Interscience, New York, 1954, pp. 43-51.

[14] M. E. Rose, Elementary Theory of Angular Momentum, Wiley-Interscience, New York, 1957, Chaps. 3 and 4.

[15] Strictly speaking, we ought to construct wave functions with definite parity. This would require us to use linear combinations of the form $F_{\Lambda}D^{J}_{M\Lambda} \pm F_{-\Lambda}D^{J}_{M-\Lambda}$ for the $^1\Pi$ state corresponding to its two Λ components. Since this procedure tends to obscure the basic photodissociation process by further burying it in sums of Clebsch-Gordan coefficients, we choose to follow a simpler course.

[16] Reference [13], pp. 685-687.

[17] B. Brehm, M. A. Gusinow, and J. L. Hall, Phys. Rev. Letters, 19, 737 (1967); J. L. Hall and M. W. Siegel, J. Chem. Phys., 48, 943 (1968); M. W. Siegel, R. J. Celotta, J. L. Hall, J. Levine, and R. A. Bennett, "Molecular Photodetachment Spectrometry I: The Electron Affinity of Nitric Oxide and the Molecular Constants of NO^-"; R. J. Celotta, R. A. Bennett, J. L. Hall, M. W. Siegel, and J. Levine "Molecular Photodetachment Spectrometry II: The Electron Affinity of O_2 and the Structure of O_2^-."

[18] U. Fano, Comments At. Mol. Phys., 2, 30 (1970); H. A. Stewart, Phys. Rev., A2, 2260 (1970).

[19] A. C. G. Mitchell, Z. Physik, 49, 228 (1928).

[20] H. G. Hanson, J. Chem. Phys., 23, 1391 (1955); ibid., 27, 491 (1957); ibid., 47, 4773 (1967).

[21] R. N. Zare and D. R. Herschbach, J. Mol. Spectry., 15, 462 (1965).

[22] V. N. Sasaki and T. Nakao, Proc. Imp. Acad. Japan, 11, 413 (1935); ibid., 17, 75 (1941).
[23] G. H. Dunn and L. J. Kieffer, Phys. Rev., 132, 2109 (1963); L. J. Kieffer and R. J. Van Brunt, J. Chem. Phys., 46, 2728 (1967); R. J. Van Brunt and L. J. Kieffer, Phys. Rev., A2, 1293 (1970).
[24] M. Leventhal, R. T. Robiscoe, and K. R. Lea, Phys. Rev., 158, 49 (1967); J. C. Pearl, D. P. Donnelly, and J. C. Zorn, Phys. Letters, 30A, 145 (1969); M. Misakian and J. C. Zorn, Phys. Rev. Letters, 27, 174 (1971).
[25] W. R. Ott, W. E. Kaupilla, and W. L. Fite, Phys. Rev., A1, 1809 (1970); D. A. Vroom and F. J. de Heer, J. Chem. Phys., 50, 580 (1969); P. J. O. Teubner, W. E. Kaupilla, W. L. Fite, and R. J. Girnius, Phys. Rev., A2, 1763 (1970); R. D. Nathan and R. C. Isler, Phys. Rev. Letters, 26, 1091 (1971).
[26] R. J. Van Brunt and L. J. Kieffer, Phys. Rev., A2, 1889 (1970).
[27] G. W. McClure, Phys. Rev., 130, 1852 (1963); D. K. Gibson and J. Los, Physica, 35, 258 (1967); D. K. Gibson, J. Los, and J. Shopman, Phys. Rev. Letters, A25, 634 (1967).
[28] F. A. Paneth and W. Hofeditz, Chem. Ber., 62B, 1335 (1929). See also E. W. R. Steacie, Atomic and Free Radical Reactions, Reinhold, New York, 1954.
[29] J. Franck, Trans. Faraday Soc., 21, 536 (1925); ibid., Z. Physik Chem., 120, 144 (1926).
[30] R. S. Mulliken, J. Chem. Phys., 4, 620 (1936).
[31] L. Mathieson and A. L. G. Rees, J. Chem. Phys., 25, 753 (1956).

Received November 8, 1971